Resonant-Tunneling-Diode Terahertz Oscillator Using Patch Antenna Integrated on Slot Resonator for Power Radiation

Kengo Okada, Kouhei Kasagi, Naoto Oshima, Safumi Suzuki, and Masahiro Asada, *Fellow, IEEE*

***Abstract*—In this paper, we proposed and fabricated resonant-tunneling-diode (RTD) terahertz oscillators integrated with slot-fed patch antennas to extract output power without using typical Si lenses. A square patch antenna with a 170 μm-long side was fabricated on a 7 μm-thick benzocyclobutene (BCB) layer stacked on an RTD with a slot resonator. The RTD oscillated at $\sim$510 GHz, and an output power of $\sim$40 μW radiated in the upward direction without the Si lens. An equivalent circuit model was proposed to estimate the output power, and the circuit parameters were derived from the calculated admittance by electromagnetic simulation. The dependence of the output power on the side length of the patch antenna agreed with the theoretical calculation. Higher output power was expected with the optimization of BCB thickness and RTD with a high current density. The radiation pattern was measured, and a directivity of 7 dBi was obtained.**

***Index Terms*—Patch antennas, resonant tunneling devices, submillimeter-wave integrated circuits.**

I. Introduction

RECENTLY, the terahertz (THz) range has received considerable attention because various applications are expected at this frequency [1]. In particular, high-capacity short-distance wireless communication using the wide band in the THz range is an important application. Demonstrations of THz communication have been intensively carried out [2]–[6]. To popularize such THz communications in the future, compact, coherent, and high-power solid-state sources, which can be installed in mobile devices, are considered to be key components. Resonant tunneling diode (RTD) is a good candidate for such sources [7]–[11] and can oscillate in the THz range with a DC bias at room temperature. We have recently achieved RTDs with a fundamental oscillation of up to 1.55 THz [11] and high output power of $\sim$610 μW at 620 GHz [12]. Demonstrations of THz communications using RTDs have been reported [5], [6].

In these oscillators, a millimeter-scale hemispherical Si lens must be placed beneath the RTD oscillator to extract output power because most of the output power is radiated into the substrate side owing to the high dielectric constant of the semiconductor substrate. Furthermore, the Si lens is bulky, and careful positioning of the RTD oscillator on the lens surface is necessary. If constructing an oscillator structure without a Si lens is possible, the RTD oscillator size can be considerably reduced. Although some structures without a Si lens have been reported for this purpose [8], [9], [13], a relatively complicated fabrication process or a precise design was required. Additionally, an impedance-matching method between the RTD and the antenna for high output power was not presented.

In the present work, we report a novel RTD oscillator to extract output power by integrating a slot-coupled patch antenna without a Si lens. The oscillation mechanism and output power extraction are explained using an equivalent circuit model. This structure can be fabricated as an extension of the previous structure that required a Si lens without a complicated process, can achieve impedance matching between the RTD and the antenna by optimizing the benzocyclobutene (BCB) thickness, and can be easily extended to a patch array for high directivity.

II. Device Structure and Fabrication Process

Fig. 1(a) shows the structure of the proposed RTD oscillator. A planar RTD oscillator with a slot resonator is fabricated on an InP substrate, and a square patch antenna is formed on a low-dielectric constant BCB layer stacked on the oscillator. The slot resonator is positioned directly underneath the center of the patch antenna. The slot and patch antennas are inductively coupled [14], and output power is obtained in the upward direction from the patch antenna. In addition, the side of the patch antenna perpendicular to the slot is designed to be approximately $\lambda/(2n_{\mathrm{BCB}})$ long to achieve resonance with the oscillation frequency, where λ is the wavelength of the oscillation frequency in free space and n_{BCB} is the refractive index of the BCB layer. Various antenna lengths of 135–203 μm were fabricated for observation of output power dependence on antenna length. The magnetic field parallel to the slot is generated by slot resonator and coupled with the patch antenna. Because the direction of the electric field in the patch antenna is perpendicular to the slot, the electric field in the patch antenna parallel to the slot is constant and resonance in this direction does not occur. The BCB layer

Manuscript received November 25, 2014; revised April 20, 2015; accepted May 29, 2015. Date of publication June 16, 2015; date of current version July 16, 2015. This work was supported in part by the Scientific Grants-in-Aid from the Ministry of Education, Culture, Sports, Science and Technology, Japan, the Industry–Academia Collaborative R&D Program from the Japan Science and Technology Agency, Japan, and the Strategic Information and Communications R&D Promotion Programme (SCOPE) from the Ministry of Internal Affairs and Communications.

K. Okada, K. Kasagi, N. Oshima, and M. Asada are with the Interdisciplinary Graduate School of Science and Engineering, Tokyo Institute of Technology, Tokyo 152-8552, Japan (e-mail: asada@pe.titech.ac.jp).

S. Suzuki is with the Graduate School of Science and Engineering, Tokyo Institute of Technology, Tokyo 152-8552, Japan (e-mail: suzuki.s.av@m.titech.ac.jp).

Color versions of one or more of the figures in this paper are available online at http://ieeexplore.ieee.org.

Digital Object Identifier 10.1109/TTHZ.2015.2441740

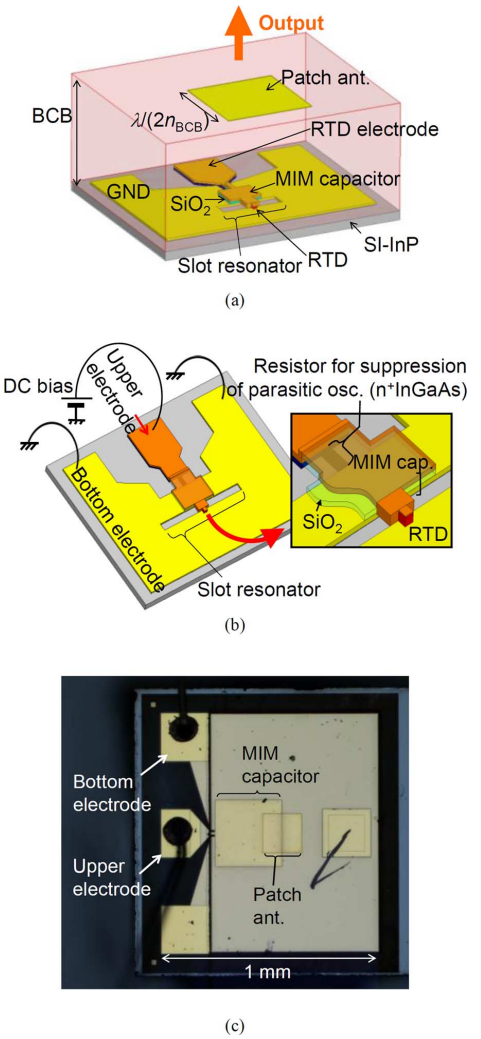

Fig. 1. Schematic structure of the RTD oscillator integrated with a patch antenna. (a) Entire structure including the RTD, slot resonator, and patch antenna on the BCB layer. (b) RTD and slot resonator on an InP substrate and their expansion. (c) Photomicrograph of the fabricated device. Although the RTD mesa and slot resonator are located at the center of the patch antenna, these structures are hidden under the patch electrode. The chip size is $\sim 1 \times 1$ mm^2.

thickness is designed to be much thinner than the oscillation wavelength (7 μm, as shown in Fig. 1).

A part of the slot resonator and RTD shown in Fig. 1(a) is magnified and shown in Fig. 1(b). An AlAs/InGaAs double-barrier RTD is located at the center of the slot resonator. The RTD has a negative differential conductance (NDC), which is utilized for THz oscillation. The peak current density is 13 mA/μm^2, and the peak-to-valley current ratio is $\sim$2. The peak and valley voltages of the RTD are 0.35 and 0.55 V, respectively. The current density and voltage width of the NDC region (ΔJ and ΔV) are 6.5 mA/μm^2 and 0.2 V, respectively. We apply a bias voltage around the center of the NDC region ($\sim$0.45 V). The area-normalized capacitance of the RTD is 14 fF/μm^2. The RTD area is 2.4 μm^2, and the slot-resonator length is 15 μm. The lower electrode of the RTD is connected to the slot edge, and the upper electrode is connected to a metal layer separated by a SiO_2 layer from the slot. Beneath this metal layer, a sheet resistor consisting of n^+-doped InGaAs is connected in parallel with the RTD to suppress parasitic oscillation due to the external circuits that include the bias line. The external circuits that includes the bias line and the n^+-InGaAs sheet resistor can be neglected because the metal-insulator–metal (MIM) capacitor is shortened to operate in the THz range. The oscillator structure shown in Fig. 1(b) is, in principle, the same as the previous structure [15] except that the direct modulation frequency limit is much higher for this structure ($\sim$30 GHz); its details will be reported [16].

The fabrication process is briefly described as follows. First, an RTD mesa is formed by depositing Ti/Pd/Au and wet chemical etching ($H_2SO_4/H_2O_2/H_2O$). A bottom electrode (Ti/Pd/Au) is then formed. These electrodes are covered with a SiO_2 film as an etching mask, and formation of the slot antenna and the device isolation are completed by reactive ion etching (CH_4/H_2) and wet chemical etching ($H_2SO_4/H_2O_2/H_2O$) using the SiO_2 mask. Contact holes are opened, and the upper metals of the MIM capacitors are formed by the deposition of Cr/Au. The bridges between the upper electrodes of the mesas and the MIM capacitors are formed by deposition of Cr/Au. From these processes, the RTD and slot resonator structure shown in Fig. 1(b) are completed. The oscillation frequencies of the fabricated devices without a patch antenna are measured at this stage. After the oscillation frequency measurement, the photo BCB dielectric layer is stacked on the device by spin coating and baking at 250 °C. Finally, the patch antenna electrode is formed by depositing Cr/Au. The side length of the patch antenna is designed using the measured oscillation frequency. Fig. 1(c) shows a photomicrograph of the fabricated device.

III. Equivalent Circuit Model and Derivation of Circuit Parameters

The equivalent circuit models shown in Fig. 2 are used to explain the operation of the oscillator shown in Fig. 1(a). The RTD and slot resonator are connected in parallel, as shown in the left-hand side of Fig. 2(a). The patch antenna is inductively coupled with the slot resonator [14]. The coupling strength depends on the magnetic field that surrounds the patch antenna. The magnetic field increases with the aperture width of the slot antenna and the distance between the slot and patch antenna. Because a separation of the coupling part admittance is difficult, we estimate the patch antenna admittance including coupling part, as shown in the right-hand side of Fig. 2(a). The detailed equivalent circuit is shown in Fig. 2(b). The parasitic elements of the RTD are neglected for simplification. The admittance viewed from A-A', which is composed of the slot resonator and patch antenna, is expressed as $Y_{\rm all}$. The patch antenna admittance (right-hand side from B-B') is expressed as $Y_{\rm patch}$.

The oscillation circuit is constructed using the RTD and slot resonator, and the patch antenna extracts the output power from this oscillation circuit. Because the LC components of the patch antenna are much smaller than those of the slot resonator and RTD, the oscillation frequency is mostly determined by the resonance frequency of the LC circuit of the RTD and the slot resonator, consisting of the capacitance of the RTD ($C_{\rm RTD}$) and the inductance and capacitance of the slot ($L_{\rm S}$ and $C_{\rm S}$), which can be changed by the antenna length. $G_{\rm S}$ indicates the power leakage from the slot resonator radiated to the substrate side due

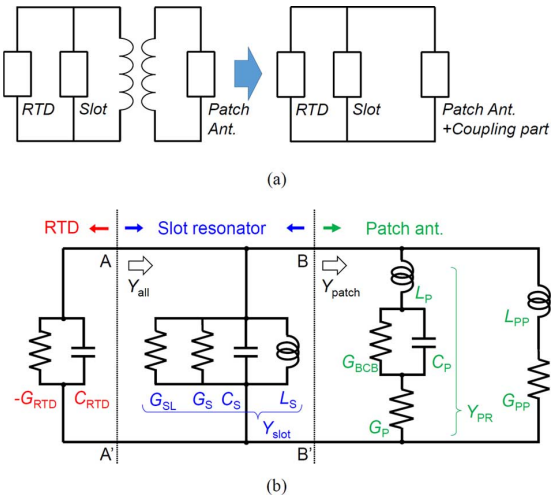

Fig. 2. Equivalent circuit of the RTD oscillator with the slot resonator and patch antenna. The left-hand side of (a) shows the model of the inductive-coupling part between the slot resonator and patch antenna, and the right-hand side shows its simplified model. (b) Detailed equivalent circuit. The parasitic elements of RTD are neglected.

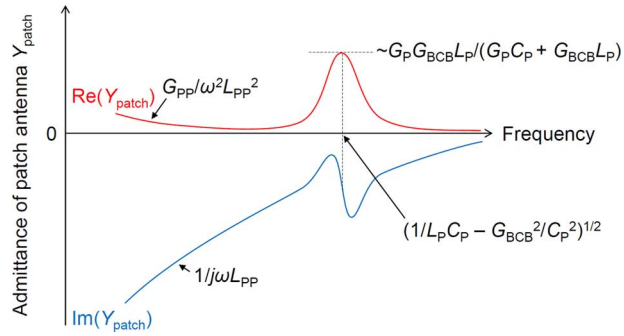

Fig. 3. Sketch of the admittance curve of the equivalent circuit model of the patch antenna as shown in Fig. 2(b). The real part of Y_{patch} has a peak at half-wave resonance of the patch antenna $(1/L_{\mathrm{P}}C_{\mathrm{P}} - {G_{\mathrm{BCB}}}^2/{C_{\mathrm{P}}}^2)^{1/2}$. The peak height is $\sim G_{\mathrm{P}}G_{\mathrm{BCB}}L_{\mathrm{P}}/(G_{\mathrm{P}}C_{\mathrm{P}} + G_{\mathrm{BCB}}L_{\mathrm{P}})$. The full width at half maximum of the resonance is determined by the Q-factor of Y_{PR}. The lower frequency characteristics are determined by G_{PP} and L_{PP} for the real part of Y_{patch} and L_{PP} for the imaginary part of Y_{patch}. From these characteristics, the circuit parameters can be derived.

to the high refractive index of the InP substrate. The conduction loss of the slot resonator is expressed as G_{SL}. Oscillations take place if the NDC of the RTD $(-G_{\mathrm{RTD}})$ compensates for the sum of the losses of the slot resonator $(G_{\mathrm{S}} + G_{\mathrm{SL}})$ and the patch antenna (real part of Y_{patch}).

The patch antenna can be considered as a microstrip line with both ends opened. Therefore, the inductance and capacitance components alternately appear with the increase in frequency in the admittance of a fixed-size patch antenna. The cycle of alternating changes corresponds to a quarter-wavelength of an electromagnetic wave. The series-connected C_{P} and L_{P} are the first and second components with increasing frequency, respectively, and their series resonance is expressed as half-wavelength resonance of the patch antenna. Electromagnetic radiation in the patch antenna occurs at half-wavelength resonance, and the radiation conductance G_{P} is thus connected in series with L_{P} and C_{P}. L_{PP} is the inductance of the coupling part. The actual circuit includes the conduction loss due to electrode G_{PP} and the BCB dielectric loss G_{BCB}. G_{PP} is connected in series with L_{PP}, and G_{BCB} is connected in parallel with C_{P}. Although the conduction loss is also connected in series with L_{P}, we found that the loss is negligible through the derivation process of circuit parameter. The real part of the whole admittance of the patch antenna has a peak G_{P} at the series resonance because the impedance of the series-connected L_{P} and C_{P} becomes zero in a lossless circuit case, i.e., without G_{PP} and G_{BCB}.

We can calculate the whole admittance Y_{all} by 3D electromagnetic simulation (ANSYS HFSS). However, to estimate the output power through the patch antenna, the circuit parameters should be separated from Y_{all}. Fig. 3 shows a sketch of the admittance curve of the patch antenna. The circuit parameters can be derived by parameter fitting using the characteristics of the patch antenna resonance and the low-frequency characteristics, as shown in Fig. 3.

The detailed method to derive the parameters of the equivalent circuit is described as follows. In this derivation process, a device with 170-μm-long patch antenna and 15-μm-long slot resonator is used for an example. First, the parameters of the slot antenna are estimated. The slot-antenna loss, which is composed of the sum of radiation conductance G_{S} and conduction loss G_{SL}, and the LC components of the slot antenna (L_{S} and C_{S}) are estimated using the calculated admittance of the structure without a patch antenna. The assumed dielectric constants for InP and BCB are 12.1 and 2.6, respectively. The $\tan\delta$ of the photo BCB with 250 °C curing in the THz range is 0.0107 [17]. The conductance of the Au electrode is 4.1×10^7 S/m. The dielectric loss of InP is small and neglected. G_{S} can be obtained from the model by changing the electrode material to a perfect conductor from Au. This method is the same as that in the previous RTD oscillator without a patch antenna and is described in [15]. The derived L_{S} and C_{S} are 3.3 pH and 2.4 fF, respectively. Although G_{S} and G_{SL} are frequency dependent, there is less than 10% variation in the 450–550-GHz range. G_{S} and G_{SL} values at 510 GHz are 0.26 and 16 mS.

The admittance of a structure with a perfect conductor electrode and BCB with zero $\tan\delta$ is simulated to derive a lossless circuit (without G_{SL}, G_{BCB}, and G_{PP}). The calculated admittance $Y_{\mathrm{patch}}(= Y_{\mathrm{all}} - Y_{\mathrm{S}})$ is shown by the solid line in Fig. 4(a). L_{PP} is estimated using the low-frequency characteristics of the imaginary part of the admittance. The resonant frequency is the LC resonance of L_{P} and C_{P}, and the full width at half maximum of the resonance is determined by the Q-factor of series connected G_{P}, L_{P}, and C_{P} $(Q = G_{\mathrm{P}}(L_{\mathrm{P}}/C_{\mathrm{P}})^{1/2})$. G_{P} is determined using the peak amplitude of the real part of the admittance. L_{P} and C_{P} are estimated by fitting with the imaginary part of Y_{patch} at around the patch resonance. The derived values of G_{P}, L_{P}, C_{P}, and L_{PP} are 17 mS, 1.2 nH, 0.078 fF, and 0.11 nH, respectively. The admittance using the equivalent circuit with the derived parameters is also shown by the dashed line in Fig. 4(a). The equivalent circuit model perfectly fits the calculated admittance using HFSS.

The next processes are the derivation of G_{PP} and G_{BCB}. The calculated admittance of the structure with conduction loss and BCB dielectric loss is indicated by the solid line in Fig. 4(b). Because the resonance frequency is slightly shifted due to the

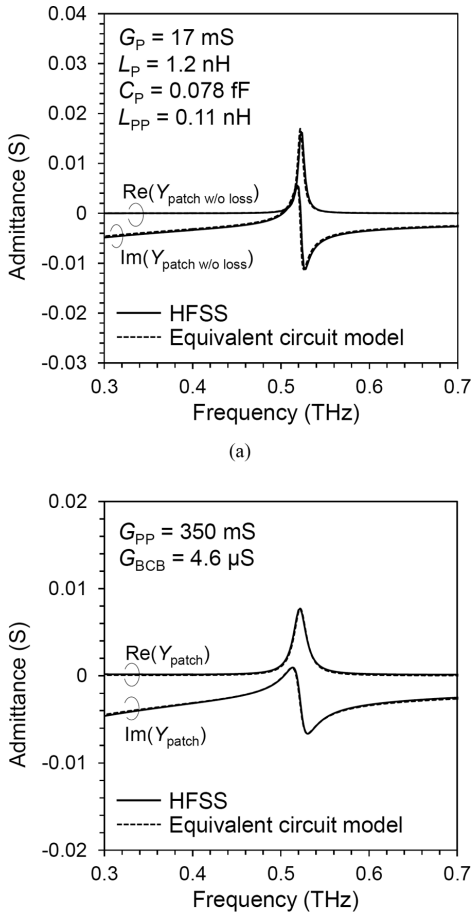

Fig. 4. Comparison between the (solid line) HFSS-calculated admittance and (dashed line) regenerated admittance using the equivalent circuit for (a) a lossless model (without $G_{\rm PP}$ and $G_{\rm BCB}$) and (b) a model that includes losses. The side length of patch antenna and slot resonator length are 170 and 15 μm. The derived parameters are shown in the inset. The equivalent circuit model well fits the curves of the HFSS simulation.

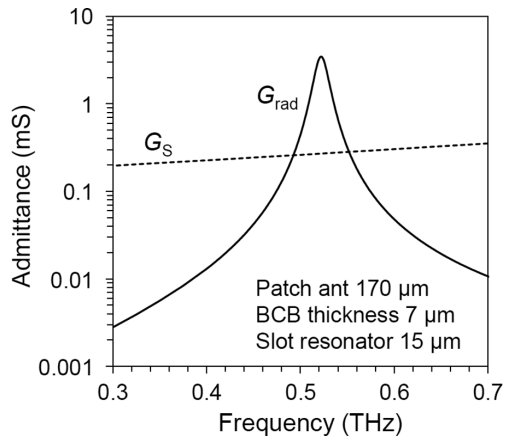

Fig. 5. Comparison between the radiation conductance values in the upward direction $G_{\rm rad}$ and substrate-side direction $G_{\rm S}$.

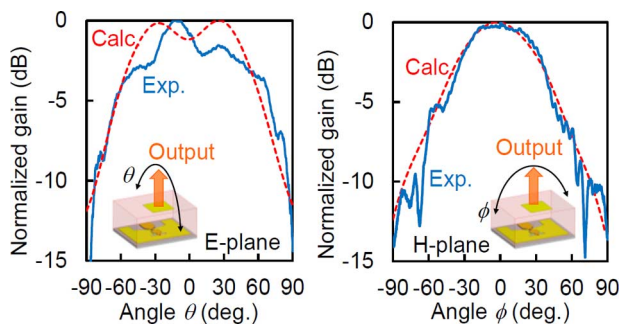

Fig. 6. Measured radiation patterns in the E- and H-planes. The patterns calculated with the electromagnetic simulator are also shown.

parallel conductance $G_{\rm BCB}$ (inset in Fig. 3), $G_{\rm BCB}$ can be estimated using the shift. $G_{\rm PP}$ is obtained by fitting the low-frequency characteristics of the real part of $Y_{\rm patch}$. The derived $G_{\rm PP}$ and $G_{\rm BCB}$ values are 350 mS and 4.6 μS, respectively. The regenerated admittance using the equivalent circuit model with the derived parameters is shown by the dashed line in Fig. 4(b). The equivalent circuit model fits well with the calculated admittance using HFSS.

The output power extracted from the patch antenna corresponds to the power consumed by $G_{\rm P}$ in the equivalent circuit, which is expressed as $1/2\times|Y_{\rm PR}|^2/G_{\rm P}\times v_{\rm osc}^2$, where $Y_{\rm PR}$ is the admittance composed of $G_{\rm P}$, $L_{\rm P}$, $C_{\rm P}$, and $G_{\rm BCB}$ and $v_{\rm osc}$ is the oscillation voltage across the RTD. The net radiation conductance $G_{\rm rad}$ can be defined as $|Y_{\rm PR}|^2/G_{\rm P}$. In actual operation, an electromagnetic wave is generated by the oscillator part (the RTD and slot resonator), stored in the cavity created by the patch antenna and BCB layer, and radiated from the patch antenna into the air. However, output power is also radiated from the slot into the substrate side, which corresponds to $G_{\rm S}$. The comparison between upward $G_{\rm rad}$ and substrate-side $G_{\rm S}$ is shown in Fig. 5. At the peak, $G_{\rm P}$ is more than tenfold than $G_{\rm S}$ by the resonance of the patch antenna; higher output power radiation to the upward side is expected around the resonance.

IV. Experimental Results and Discussion

The measured and simulated radiation patterns in the E- and H-planes are shown in Fig. 6 for a device with a patch antenna with a 170-μm-long side. The device was mounted on a glass slide and wire bonded [Fig. 1(c)], and the radiation pattern was measured by rotating the device. In the measurements, a liquid-He-cooled Si-composite bolometer, which was calibrated by Ericson power meter (PM3), was used as the detector. Although the device can be oscillated in a continuous-wave mode, the measurements were performed in the pulsed mode using a lock-in technique to eliminate surrounding noise. The distance between the device and the bolometer was set to 20 cm. An iris diaphragm with a narrow aperture was inserted in front of the bolometer window to provide a high angular resolution of 2°. In this measurement, electromagnetic wave absorbers were not employed. The multiple reflection between the iris diaphragm and the device was probably weak, because the measurement distance was long. Therefore, the improvement in radiation pattern measurement by the absorber attached to the iris diaphragm is considered to be small. The transmission loss due to absorption in the atmosphere is negligible because the oscillation frequency of 500 GHz is in the low-loss range. The output power was normalized using the peak power. The noise level was below −20 dB. We repeatedly measured the radiation pattern. The fluctuation between measurements was small at

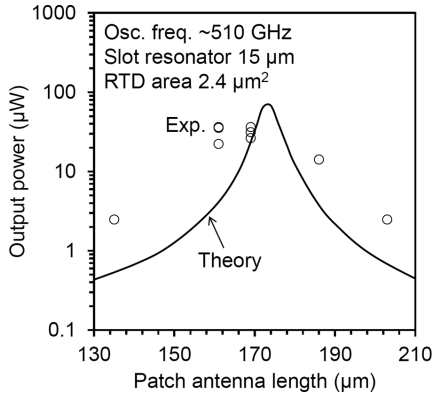

Fig. 7. Dependence of the output power on the side length of the patch antenna. To estimate the theoretical output power under various antenna lengths, the circuit parameters for each antenna length are estimated using the derivation method described in Section III.

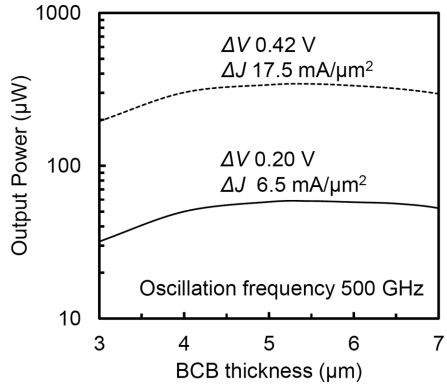

Fig. 8. Theoretical output power as a function of the BCB thickness for various RTDs. The output power is roughly maximized at around a BCB thickness of 5-6 μm. A high output power ($> 300\ \mu$ W) is expected with an RTD with a large NDC region.

2%–3%. The pattern in the H-plane had a single peak, whereas that in the E-plane had a double peak because the slot antenna is not an ideal point source for the patch antenna. The measured pattern in the H-plane agreed well with the calculated pattern, whereas that in the E-plane did not agree, probably because of the surface roughness and steps on the BCB layer and patch antenna, although the reason for this discrepancy is not yet clear at the moment. The antenna directivity was $\sim$7 dBi in the upward direction and can be increased by extending the patch antenna to its array on the surface of the BCB layer.

Fig. 7 shows the experimental output power radiated upward as a function of the side length of the patch antenna. Because the radiation pattern was fitted with the calculation, we roughly estimated the output power by integration of the calculated radiation pattern with a normalization using the experimental power density at $\theta = 0^\circ$ and $\phi = 0^\circ$. The maximum output power obtained in the experiment was $\sim$40 μW at side lengths of 160 and 170 μm. The theoretical output power was calculated using the derived parameters with the method in [15] and is also shown in Fig. 7. The calculated output power was maximum at a side length of 175 μm, exhibiting the resonance of the patch antenna. The theoretical output power was consistent with the experiments. The theoretical peak was slightly shifted from the experimental peak, probably because the used BCB dielectric constant in the calculation was different to the actual dielectric constant.

The output power radiated into the substrate side was measured by mounting the device on a Si hemispherical lens. The output power through the lens was collected by a large parabolic mirror (diameter of $\sim$10 cm). However all of the output power cannot be collected, therefore, we thus estimated the output power by assuming a radiation pattern of ideal slot antenna. The percentage of collected power with parabolic mirror was $\sim$20%. Around 10 μW was obtained, which was independent of the size of the patch antenna. This is because $G_{\rm S}$ was independent on the side length of the patch antenna and the electric field of the substrate side is unchanged by the integration of the patch antenna. We also measured the output power of the device before integration of BCB layer and patch antenna with same method as shown above. The output power was unchanged by patch antenna integration. The ratio of the power in the substrate direction to that in the upward direction was 1:4 for the patch antenna with a 170 μm-long side. Relatively high output power was extracted in the upward direction without a Si lens.

The oscillation spectra were measured by a Fourier-transform infrared spectrometer. Although oscillators with various patch antenna lengths were fabricated, oscillation frequencies for these oscillators were almost same around 510 GHz. The distribution of oscillation frequency was 2%–3%. The frequency change after the integration of the patch antenna was within $\sim$2%, and the oscillation frequency was almost independent of the side length of the patch antenna.

High output power can be obtained using a large-area RTD and by impedance matching between the RTD and the load conductance [15], i.e., the output power can be maximized if the matching condition $\mathrm{Re}(Y_{\rm all}) = G_{\rm RTD}/2$ is satisfied, as shown in Fig. 2, which is possible by adjusting the BCB thickness. This method corresponds to that of the offset-fed slot antenna [12]. Fig. 8 shows the theoretical output power as a function of the BCB thickness for RTDs with various ΔJ and ΔV. Because the oscillation and resonance frequencies of the patch antenna are slightly shifted when the BCB thickness is varied, the side length of the patch antenna and mesa area are adjusted in this calculation to maintain the oscillation and resonance frequencies at 500 GHz. Fig. 8 shows that the output power is maximized at an optimum thickness of $\sim$5–6 μm, which corresponds to the impedance-matching point. With this adjustment, high output power and its high ratio with respect to that in the substrate side can be obtained.

A high antenna gain can be achieved using a collimation-type Si lens. However, the experimentally obtained antenna gain of the single patch antenna configuration is not very high at $\sim$7 dBi. The patch antenna array is effective for high antenna gain. In this case, the patch antenna elements are connected to one another by a microstrip line. Owing to the transmission loss of the microstrip line, the increment in the antenna gain due to the array configuration gradually decreases with increasing array elements. Because the transmission loss of the thin-film microstrip line with BCB is $<$ 1 dB/mm, the transmitted power becomes half by $\sim$3 mm transmission and the limit of the area of the antenna array will be $<$ 10 mm^2. Although the patch antenna array is not effective compared to the large size Si lens ($>$ 10 mm^2), this is probably enough for installing in mobile devices.

V. Conclusion

In conclusion, we have proposed and fabricated RTD THz oscillators integrated with slot-fed patch antennas to extract output power without using typical Si lenses. A square patch antenna with a 170 μm-long side was fabricated on a 7 μm-thick BCB layer stacked on an RTD with a slot resonator. The RTD oscillated at 510 GHz, and output power of $\sim$40 μW radiated in the upward direction without the Si lens. The equivalent circuit model was proposed to estimate the output power, and the circuit parameters were derived using the calculated admittance by electromagnetic simulation. The dependence of the output power on the side length of the patch antenna agreed with that derived from the theoretical calculation. The radiation pattern was measured, and a directivity of 7 dBi was obtained. Further, a higher output power can be expected by optimizing the BCB thickness and the RTD with high current density. With this structure, a compact oscillator without a Si lens can be possibly fabricated using RTDs.

Acknowledgment

The authors would like to thank Prof. Emer. Y. Suematsu and Prof. Emer. K. Furuya of the Tokyo Institute of Technology for their continuous encouragement. The authors would also like to thank Prof. S. Arai and Prof. Y. Miyamoto and Assoc. Prof. M. Watanabe and Assoc. Prof. N. Nishiyama of the Tokyo Institute of Technology for the fruitful discussions and encouragement.

References

[1] M. Tonouchi, "Cutting-edge terahertz technology," *Nat. Photon.*, vol. 1, pp. 97–105, 2007.
[2] T. Nagatsuma *et al.*, "Terahertz wireless communications based on photonics technologies," *Opt. Express*, vol. 21, no. 20, pp. 23736–23747, Sep. 2013.
[3] S. Koenig *et al.*, "Wireless sub-THz communication system with high data rate," *Nat. Photon.*, vol. 7, pp. 977–981, Oct. 2013.
[4] G. Ducournau *et al.*, "Ultrawide-bandwidth single-channel 0.4-THz wireless link combining broadband quasi-optic photomixer and coherent detection," *IEEE Trans. THz Sci. Technol.*, vol. 4, no. 3, pp. 328–337, Mar. 2014.
[5] K. Ishigaki, M. Shiraishi, S. Suzuki, M. Asada, N. Nishiyama, and S. Arai, "Direct intensity modulation and wireless data transmission characteristics of terahertz-oscillating resonant tunnelling diodes," *Electron. Lett.*, vol. 48, no. 10, pp. 582–583, 2012.
[6] T. Shiode, T. Mukai, M. Kawamura, and T. Nagatsuma, "Giga-bit wireless communication at 300 GHz using resonant tunneling diode detector," in *Proc. Asia-Pacific Microw. Conf.*, Melbourne, Australia, 2011, pp. 1122–1125.
[7] M. Reddy *et al.*, "Monolithic Schottky-collector resonant tunnel diode oscillator arrays to 650 GHz," *IEEE Electron Device Lett.*, vol. 18, no. 5, pp. 218–221, May 1997.
[8] M. Feiginov, C. Sydlo, O. Cojocari, and P. Meissner, "Resonant-tunnelling-diode oscillators operating at frequencies above 1.1 THz," *Appl. Phys. Lett.*, vol. 99, p. 233506, Dec. 2011.
[9] Y. Koyama, R. Sekiguchi, and T. Ouchi, "Oscillations up to 1.40 THz from resonant-tunneling-diode-based oscillators with integrated patch antennas," *Appl. Phys. Express*, vol. 6, p. 064102, May 2013.
[10] H. Kanaya, R. Sogabe, T. Maekawa, S. Suzuki, and M. Asada, "Fundamental oscillation up to 1.42 THz in resonant tunneling diodes by optimized collector spacer thickness," *J. Infrared, Millim. THz Waves*, vol. 35, no. 5, pp. 425–431, May 2014.
[11] T. Maekawa, H. Kanaya, S. Suzuki, and M. Asada, "Frequency increase in terahertz oscillation of resonant tunnelling diode up to 1.55 THz by reduced slot-antenna length," *Electron. Lett.*, vol. 50, no. 17, pp. 1214–1216, Aug. 2014.
[12] S. Suzuki, M. Shiraishi, H. Shibayama, and M. Asada, "High-power operation of terahertz oscillators with resonant tunneling diodes using impedance-matched antennas and array configuration," *IEEE J. Sel. Topics Quantum Electron.*, vol. 19, no. 1, Jan./Feb. 2013, Art no. 8500108.
[13] K. Urayama, S. Aoki, S. Suzuki, M. Asada, H. Sugiyama, and H. Yokoyama, "Sub-terahertz resonant tunneling diode oscillators integrated with tapered slot antennas for horizontal radiation," *Appl. Phys. Express*, vol. 2, no. 4, p. 044501, Apr. 2009.
[14] M. Himdi, J. P. Daniel, and C. Terret, "Transmission line analysis of aperture-coupled microstrip antenna," *Electron. Lett.*, vol. 25, no. 18, pp. 1229–1230, Aug. 1989.
[15] M. Asada, S. Suzuki, and N. Kishimoto, "Resonant tunneling diodes for sub-terahertz and terahertz oscillators," *Jpn. J. Appl. Phys.*, vol. 47, no. 6, pp. 4375–4384, 2008.
[16] Y. Ikeda, S. Kitagawa, K. Okada, S. Suzuki, and M. Asada, "Direct intensity modulation of resonant-tunneling-diode terahertz oscillator up to $\sim$30 GHz," *IEICE Electron. Exp.*, vol. 12, no. 3, pp. 1–10, Jan. 2015.
[17] E. Perret, N. Zerounian, S. David, and F. Aniel, "Complex permittivity characterization of benzocyclobutene for terahertz applications," *Microelectron. Eng.*, vol. 85, pp. 2276–2281, Jul. 2008.

Kengo Okada received the B.E. degree in electrical and electronic engineering from the Tokyo Institute of Technology, Japan, in 2012, where he is currently working toward the M.E. degree in electronics and applied physics, studying THz oscillating devices using resonant tunneling diodes.

Kouhei Kasagi is currently working toward the B.E. degree in electrical and electronic engineering at the Tokyo Institute of Technology, Japan, studying THz oscillating devices using resonant tunneling diodes.

Naoto Oshima received the B.E. degree in Information and Electronic System Engineering from the Sendai National College of Technology, Japan, in 2014, and is currently working toward the M.E. degree in Electronics and Applied Physics at the Tokyo Institute of Technology, Japan, studying THz oscillating devices using resonant tunneling diodes.

Safumi Suzuki received the B.E. degree in electrical and electronic engineering and the M.E. and D.E. degrees in electronics and applied physics from the Tokyo Institute of Technology, Japan, in 2005, 2007, and 2009, respectively.

From 2009 to 2014, he was an Assistant Professor in the Department of Electronics and Applied Physics, Tokyo Institute of Technology and has been an Associate Professor in the Department of Physical Electronics since 2014. He is currently engaged in research on THz electron devices.

Dr. Suzuki is a member of the Japan Society of Applied Physics (JSAP) and the Institute of Electronics, Information and Communication Engineers (IEICE) of Japan.

Masahiro Asada (F'12) received the B.E., M.E., and D.E. degrees in Physical Electronics from the Tokyo Institute of Technology, Japan, in 1979, 1981, and 1984, respectively.

In 1984, he joined the Department of Physical Electronics, Tokyo Institute of Technology as a Research Associate. From 1986 to 1987, he was with the Physics Institute of Stuttgart University, Stuttgart, Germany, as a Research Fellow of the Alexander von Humboldt Foundation. From 1988 to 1999, he was an Associate Professor in the Department of Electrical and Electronic Engineering, Tokyo Institute of Technology, and since 1999, he has been a Professor in the Interdisciplinary Graduate School of Science and Engineering. His current interests are in high-frequency electron devices, especially THz devices using nanostructures.

Dr. Asada is a Fellow of the Institute of Electronics, Information and Communication Engineers (IEICE) of Japan and the Japan Society of Applied Physics (JSAP).